Analysis of hygral induced crack growth in multiphase materials

H. Sadouki* and J.G.M. van Mier
Delft University of Technology, Faculty of Civil Engineering, Stevin Laboratory, P.O. Box 5048, 2600 GA Delft, The Netherlands

In this paper a numerical model for simulating crack growth processes caused by moisture movement in a porous multiphase material like concrete is proposed. In the model, the material is schematized as a regular triangular network of beam elements. The meso-material structure of the material is projected on top of the lattice and different properties are assigned to the different phases. In the hygral analysis the lattice elements are considered conductive pipes. In the mechanical analysis, the lattice elements are beams which are characterised by a modulus of elasticity, Poisson's ratio, tensile strength and fracture energy. In contrast to the previously developed lattice model by Schlangen & Van Mier 1992, a softening relationship was used in the fracture analysis. Examples of shrinkage cracking in normal concrete containing dense natural aggregates and in lightweight concrete containing low modulus impermeable aggregate particles are given. Moreover, a comparison between a continuum based hygral/ mechanical approach and the lattice type model is presented. The model seems a useful tool for estimating the effect of hygral shrinkage cracking on the mechanical properties of concrete.

Key words: **concrete, cracking, lattice model, transient moisture flow, shrinkage**

1 Introduction

Concrete is a brittle particle composite. The cement matrix which binds together the aggregates is highly porous, and moisture movement in the matrix may lead to shrinkage or swelling. In normal concrete, the dense natural aggregates restrain the shrinkage of the cement matrix. Unavoidably, this will lead to tensile and compressive stress concentrations in the material. Tensile stresses may lead to crack nucleation and growth, and the mechanical properties of the composite may be affected. The mechanical and fracture behaviour of concrete composites can be modelled at different levels. In the past few decades, a macroscopic approach was followed in most cases. Macroscopic non-linear fracture mechanics models were developed (for example Hillerborg et al. 1976 Bažant & Oh 1983) and have been implemented in macroscopic finite element codes, for exampleDIANA In such macro-level approaches, no internal structure of the material is considered and all non-linear effects from cracking must be included in the fracture law. However, with the further development of digital computer technology, the fracturing of the material can also be considered at other levels of observation, for example the meso-level (e.g. Roelfstra et al. 1985, Schlangen & Van Mier 1992). In the meso-level approach to fracture, the internal particle structure of concrete is included directly in the finite element model. For example Roelfstra et al. developed a

* On leave from ETH-Hönggerberg, CH-8093 Zürich, Switzerland.

numerical concrete model where the aggregate and matrix elements were modelled using conventional triangular continuum finite elements. The interface between the aggregates and matrix was modelled by means of discrete interface elements. Both tensile softening and frictional slip were possible along the interface. A different and quite promising model for simulating crack growth was introduced recently, namely the lattice approach. In lattice type models, the continuum idea is left, and the material is schematised as a network of brittle breaking beam elements. The particle structure of the concrete is projected on top of the lattice, and different properties are assigned to different beams falling in different places of the particle structure. In general three phases are recognised: interface beams, aggregate beams and matrix beams. The lattice approach was originally developed by statistical physicists, and – in modified form – applied successfully to simulating crack growth in concrete and rock by Schlangen and Van Mier (1992).

Because of the large sensitivity of porous cement composites to moisture flow and shrinkage and swelling, it was considered essential to extend the models to incorporate eigen-stresses from drying and swelling. The transient moisture flow module available in DIANA was adapted to the lattice approach. The lattice elements are in that case considered as conductive pipes. After a transient flow analysis, a fracture analysis is carried out. To this end the hygral stress distribution must be computed, and incorporated in the fracture analysis. This paper follows earlier work at the macro- and meso-level (Sadouki & Van Mier 1996a,b). In the first paper, cracking and delamination of repair layers on a concrete substrate was studied, whereas in the second paper the transient flow model was incorporated in the lattice model. In the present paper, hygral crack growth is modelled at the meso-level by means of the lattice technique. In order to allow for easier coupling to the transient moisture flow analysis available in the finite element package DIANA, the lattice analyses were performed by adopting a softening type fracture law for the lattice beams. In the earlier lattice model, brittle fracture was simulated by removing the beams directly from the lattice as soon as the tensile strength of the beam was exceeded (Schlangen & van Mier 1992). In the present approach, the complete model is contained within the DIANA environment, which is considered more practical. In the paper the complete procedure including hygral moisture flow analysis, analysis of hygral stresses, and crack grow analysis are outlined. Examples of hygral crack growth in normal gravel concrete and lightweight concrete are presented. Moreover, a comparison is made between the continuum and lattice approaches to combined moisture flow/crack growth analysis. All analyses have been carried out using two different composite structures in combination with a regular triangular lattice that will be presented first.

2 Computer generated composite structures

Concrete is a multiscale particle composite. The particles are bonded together by means of a hydraulic cement. In order to model transient moisture flow at the meso-level, a computer generated particle distribution was used. The method described in Schlangen (1993) was adopted. In Figure 1 the two different particle structures with the lattice overlay are shown. The structure of Figure 1a contains 29 % aggregates, the second structure (Figure 1b) contains 45.25 % of particles. A lower cut off for the particle size was made at 2 mm, which was done for computational reasons.

In the present analyses the length of the beams(fracture)/pipes(flow) in the regular triangular lattice was equal to 1 mm, whereas all other properties were kept as in earlier papers (see for example the overview in Van Mier et al. 1995).

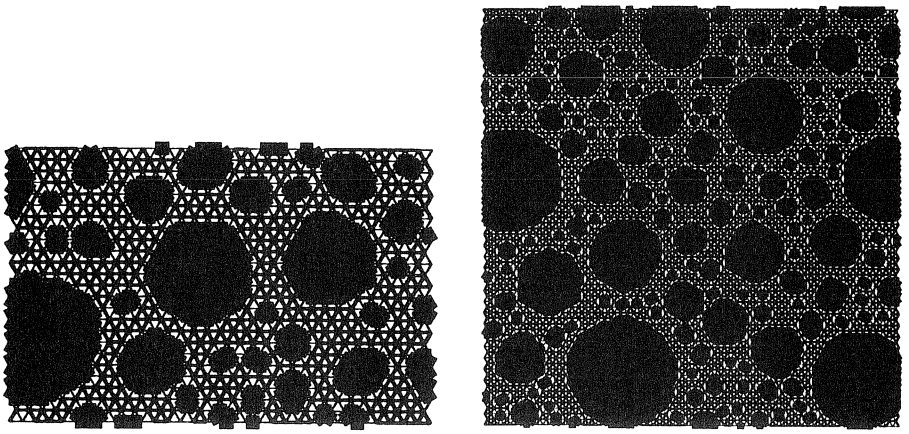

(a) (b)

Fig. 1. Computer generated particle structures with three phases: aggregate (black), interfaces and matrix. The aggregates in the figures have been filled in to better distinguish them. The lattice overlay can be seen from these figures as well. The structure in Figure (a) contains 29 % of aggregates, the second structure in Figure (b) contains 45.25 % of aggregates.

3 Transient moisture flow analysis

Moisture flow in porous materials like concrete is a highly complex process including surface absorption on the pore walls, capillary condensation, gas phase flow, surface flow and liquid flow (Quenard and Sallee 1992). In the present approach, all phenomena are described by means of a single flow equation, i.e. the different processes are not separated. The transient flow analysis is in fact a discretization of the continuum flow analysis that is available in DIANA (1996). The potential flow between two neighbouring nodes in the lattice is lumped along the line connecting the two nodes. The governing equation is:

$$\frac{\partial h}{\partial t} = div[\, D(h) \cdot \nabla h \,] \tag{1}$$

where h is the moisture potential and $D(h)$ is the moisture dependent diffusivity. In the examples given in this paper two different boundary conditions were adopted, namely,

(i) convective boundaries, with

$$q = \beta \cdot (h_s - h_{ext}) \tag{2}$$

in which β is the hygral convection coefficient, h_{ext} is the Relative Humidity of the surrounding atmosphere, and h_s is the Relative Humidity on the exposed surface.

(ii) fixed boundary potential,

$$h_s = h_{ext} \tag{3}$$

which implies that the nodes on the exposed surface are given an imposed Relative Humidity, which is equal to the external.

In Figure 2 the computed moisture distribution is shown at four different times for the composite structure of Figure 1a. The upper surface is in contact with the atmosphere, and boundary condition Eq. (2) is assumed, i.e. convection occurs. The left, right and bottom surface are sealed and assumed to be impermeable. As far as the diffusivity of the material constituents is concerned, it is assumed that the particles are impermeable, whereas the interface beams have a moisture diffusivity which is five times larger than the matrix diffusivity. This assumption is made on the basis of the fact that the interface in normal gravel concrete is normally a very open porous zone, e.g. Scrivener 1989.

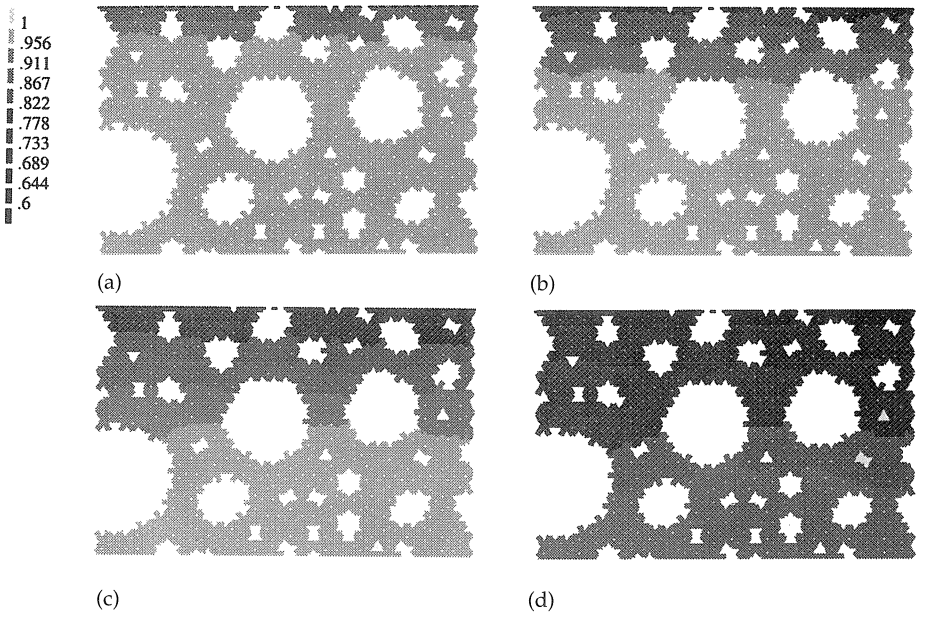

Fig. 2. Moisture distribution in the composite structure of Figure 1a at four different times of drying, i.e. t = 1, 3, 7 and 30 days (Figures (a) - (d) respectively).

It should be mentioned here that the absolute values of the diffusion coefficients are not very important. Instead, the ratios of the different diffusivities is more important. This holds for the mechanical analysis as well (Van Mier et al. 1995). At the beginning of the analysis it is assumed that both the matrix and the interface are fully saturated (100 %). The Figures reveal a gradual drying of the composite, starting from the upper edge of the mesh. The lighter grey shades in these figures indicate a high H, the darkest grey $H = 60$ %. After 30 days of drying a state of equilibrium has almost been reached.

The second example of moisture flow concerns the structure of Figure 1b. In Figure 3, the moisture distribution of the composite structure is shown at four different drying times, i.e. 1, 3, 7 and 30 days. In this example the boundary condition eq. (3) has been imposed, i.e. a fixed boundary potential of 60 % has been assumed. In this second example drying occurs at the top and bottom surfaces, whereas the left and right sides are considered completely impermeable. As far as the material is concerned, again the aggregates are assumed to be impermeable as well. The interface between aggregate and matrix, and the matrix itself are assumed to have the same diffusivity.

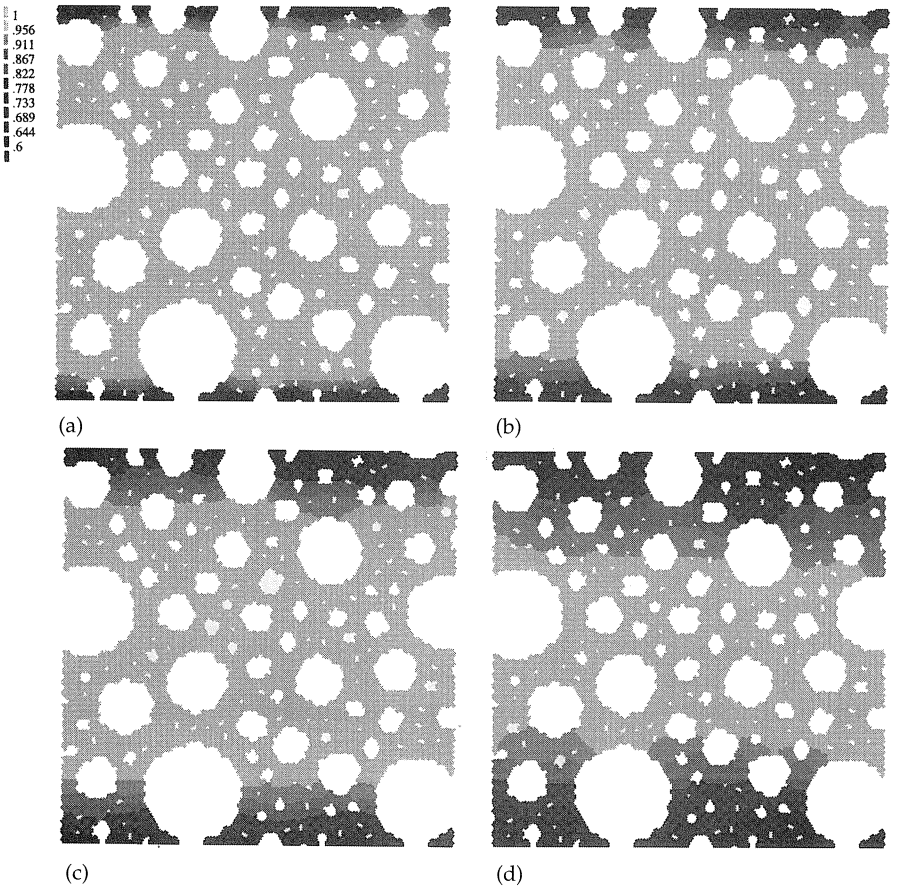

Fig. 3. Moisture distribution in the composite structure of Figure 1b at four different drying times, i.e. t = 1, 3, 7 and 30 days (Figures (a) - (d) respectively).

Comparison of the results in Figure 2 and 3 shows that the initial drying (after t = 1 day) at the free surfaces in the second analysis is much faster than in the first example. The reason is that a fixed boundary potential, as was used in the second example, is equivalent to a very high (infinite) convection coefficient. Moreover, a comparison of the two examples show that the drying out of the core of the specimen proceeds at a faster rate in the first example. Two reasons are held responsible for this, namely the lower interface diffusivity in the second example, as well as the fact that the second structure contains a larger amount of impermeable inclusions. In Sadouki & Van Mier (1996b), the model is explained in more detail and other examples are included. Using the same approach, thermal and gas transfer can be analyzed as well. These processes are governed by the same type of equations.

4 Hygral stresses

Hygral gradients were considered as the single driving force for crack propagation. In an earlier paper, the fracturing of a repair mortar overlay on a concrete substrate was analyzed using the DIANA continuum approach, see Sadouki & Van Mier 1996a. Due to drying of the material, shrinkage strains occur, which may – if restrained – lead to local tensile stress-concentrations. The shrinkage strain can be computed following

$$\Delta\varepsilon_{sh} = \alpha_{sh} \cdot \Delta h \tag{4}$$

where $\Delta\varepsilon_{sh}$ is the unrestrained hygral shrinkage, and α is the so-called shrinkage coefficient. The coefficient α depends on the composition of the material and the humidity. For $0.6 < RH < 1.0$, α is constant, see Martinola & Wittmann 1995.

Generally, however, shrinkage is restrained in concrete materials and structures. In structures, local hygral gradients caused by non-uniform drying may occur. This example was studied in Sadouki & Van Mier 1996a. In the material itself, the presence of aggregates, and/or hygral incompatibility between the different phases in the material, may cause disturbances in the stress field. In a linear elastic stress analysis, the stress-distribution in the structure of Figure 1a was estimated. The stresses were computed following,

$$\sigma = E\alpha_{sh}\Delta h \tag{5}$$

where E is the Young's modulus of the material. In the analysis, different elastic and shrinkage properties are assigned to the matrix, interface and aggregate phases. For the Young's modulus, the values are 70, 12 and 20 GPa for the aggregates, interface and matrix phases respectively. The Poisson's ratio of the lattice beams was set at 0.2 for all three phases, whereas the hygral shrinkage coefficient was assumed to be constant for the humidity interval considered, and values of α_{sh} = 0, 0.002 and 0.001 mm/(mm·h) were used for the aggregate, interface and matrix phases respectively. The drying proceeds similar as shown before in Figure 2 (where however the interface diffusivity was different from the present example). The linear elastic stresses are shown in Figure 4,

at three different drying times, viz. t = 0.25, 7 and 30 days. As the drying front advances from the top to bottom, tensile stresses develop in the matrix and interface zones, whereas the aggregates are gradually compressed. After an advanced drying time, the meso-structure of the concrete is revealed in the stress diagram of Figure 4c. The graphical representation shows aggregates that are all compressed as dark grey, whereas the tensile stresses in the matrix are shown with a lighter grey. The deformed shape of the element mesh is shown in Figure 5 at t = 1 and 7 days. Shrinkage strains are largest at the top surface which is exposed to drying. A-symmetric deformations occur because of the heterogeneity of the material. The total length change along the top surface is plotted as a function of drying time in Figure 6. A smooth curve is obtained because no cracks are allowed to develop. The stress distributions in Figure 4 already reveal that cracking must occur. Tensile stresses up to 13 MPa occur after 30 days of drying, which is considerably larger than the matrix and interface strength. Therefore a crack growth mechanism must be included in the model.

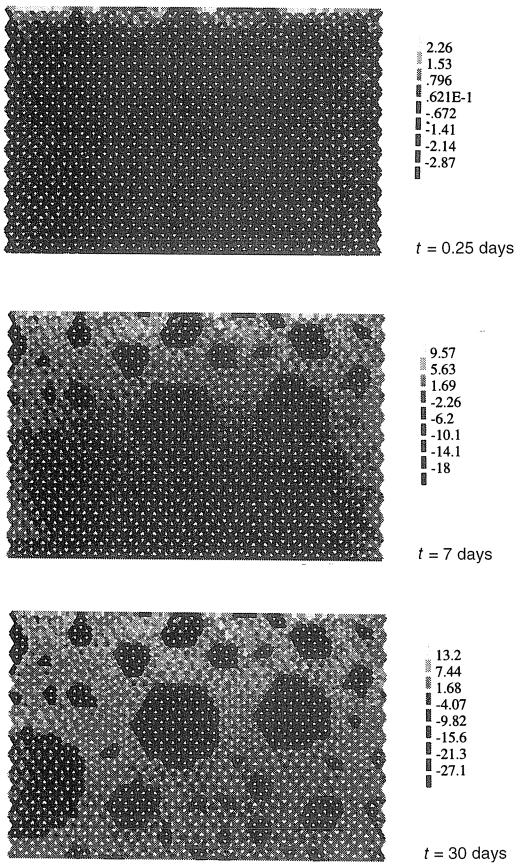

Fig. 4. Linear elastic stress analysis with the lattice model. The hygral stress distribution is shown at three different drying times, t = 0.25, 7 and 30 days. A representative drying history was shown in Fig. 2.

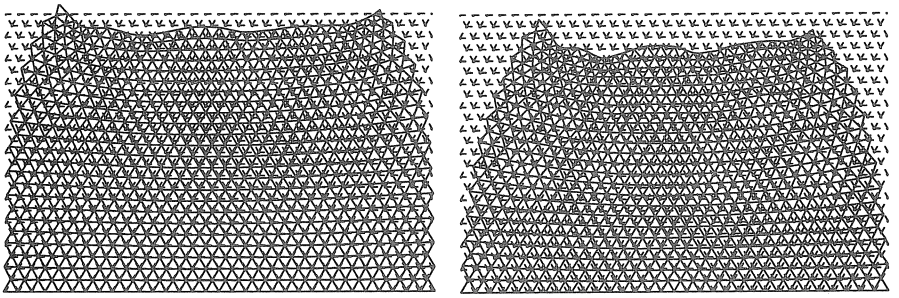

(a) (b)

Fig. 5. Deformed shapes of the composite structure of Figure 1a under hygral gradients. Two different drying times are shown, namely t = 1 day and t = 7 days. The deformations are shown enlarged, i.e. a magnification factor of 3000 was used in Figure (a), whereas for Figure (b) the deformations are magnified by a factor 1500.

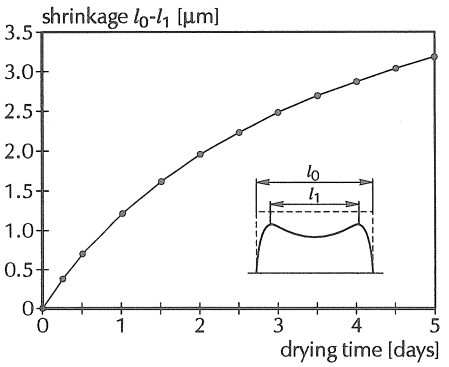

Fig. 6. Total shrinkage deformations along the top surface for the linear elastic stress analysis of Fig. 4.

5 Hygral shrinkage cracking: continuum modelling versus lattice

In the first version of the lattice model (Schlangen & Van Mier 1992), crack growth was simulated by removing a beam from the lattice as soon as the tensile stress in that beam exceeded the strength of the beam. In this way a brittle fracture was achieved. Thus, contrary to macroscopic fracture models for concrete no softening law was used. All non-linearity in the macroscopic stress-crack opening diagram of concrete in tension and shear was assumed to result from crack nucleation and growth at the particle level of the material. Therefore, including the meso-structure of the concrete was an essential part of the model. The fracture patterns simulated with the lattice model were quite realistic, but the stress-deformation response was generally too brittle, see for example in Van Mier et al. 1995. Several reasons were given for the extreme brittleness of the model such as neglecting the finest particles in the mesh, as well as by neglecting 3D-effects. In a later version of the model, it was tried to overcome the brittleness problem by removing a beam not immediately, but rather to

allow for a stepwise reduction of the beam stiffness before it was removed completely, Arslan et al. 1995. In that case more ductile stress-deformation diagrams were computed, but of course the problem is then to decide what the exact fracture law should be. In this paper a softening fracture law for the beams has been used. It was more convenient to choose this approach because the hygral flow analysis was carried out in the finite element package DIANA. There also different type of softening models are available. In the analyses shown below, a linear softening law was adopted with an extremely low fracture energy, namely $G_f = 3.75$ N/m for the matrix material, and 1 N/m for the interface zone. Because a softening fracture law is used, the computation becomes non-linear. This may cause numerical errors, which are normally circumvented in the original brittle lattice model. It should be mentioned however that with an extreme steep softening branch, salient mechanisms such as non-uniform opening in a uniaxial tension test and the development of interacting overlapping cracks can be simulated as well, see Van Mier 1986. Before embarking on a more detailed study of the effect of material composition on hygral shrinkage cracking, first a comparison will be made between a continuum (smeared) fracture model which is available in DIANA, and the "softening" lattice model as described above.

The comparison has been made on the basis of the simplified particle model of Figure 7. Three rigid inclusions are embedded in a matrix. The diffusivity of the aggregates is zero, whereas the diffusivity of the interface is twice as large as that of the matrix material. Again, the absolute values are not very important. They merely decide the duration of the drying process. In the continuum analysis, 3 noded triangular plane stress elements (464 elements) are used, which are standard available in DIANA. In the lattice analysis, the two noded beam elements with 3 DOF per node were used (727 beams). A linear softening diagram was used in both cases, with an extremely steep slope of the softening diagram as explained above. The mechanical properties are summarized in Table 1. It should be mentioned that for the continuum analysis as well as for the lattice analysis, the Young's modulus and tensile strength of both the interface and the matrix material were given a normal distribution. The scatter is given in parenthesis.

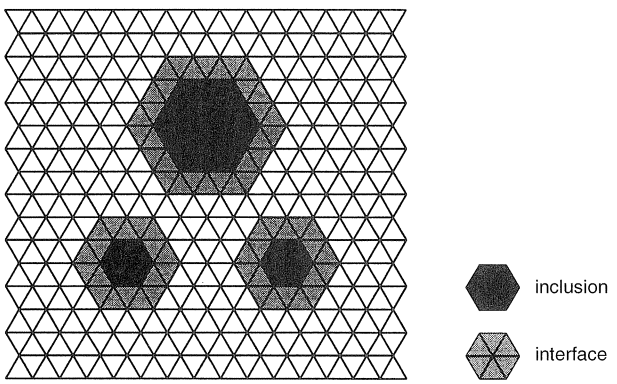

Fig. 7. Simplified three particle structure for comparison of smeared crack analysis and the lattice analysis. The upper surface of the structure is in contact with an atmosphere of 60 % RH, the other three sides are sealed.

Table 1. Mechanical properties for the fracture analysis of the three particle structure.

	E [GPa]	υ [-]	α_{sh} [mm/(mm·h)]	f_t [MPa]	G_f [N/m]
aggregate	70 (-)	0.2	0.0	7.0	-
interface	12 (3)*	0.2	0.004	1.0 (0.25)	1.0 (0.0)
matrix	20 (4)	0.2	0.002	4.5 (1.5)	3.75 (0.0)

* values between parenthesis indicate the scatter of a given property.

The analyses are now performed as follows. In the continuum analysis, first a flow analysis is carried out (the normal module available in DIANA), whereafter the hygral stresses are computed. Following this a smeared cracks analysis is carried out, which is also standard available in DIANA. For the lattice analysis, a newly implemented "pipe" element was used for the moisture analysis, hygral stresses were computed in the pipe/beams, and next a softening fracture analysis was carried out within the framework of DIANA. Thus, the main difference between the two approaches is the discrete character of the lattice approach. It should be mentioned however that, because it was decided to perform the entire computation within the DIANA framework, a softening fracture law had to be used for the lattice analysis as well. The removal of the beams, as normally done in lattice analysis, can not be handled in DIANA. This option will however be built in the programme in the very near future. For the hygral analysis, it was assumed that drying can occur only along the upper edge of the structure of Figure 7, which is exposed to 60 % RH. All other sides are sealed and assumed to be completely impermeable. Again the matrix and interface are assumed to be completely saturated at the beginning of the analysis, whereas the aggregates are assumed to be impermeable (see also Table 1). The good agreement between the continuum and lattice approach to moisture transport was shown in an earlier paper (Sadouki & Van Mier 1996b). At that time the mechanical analysis was not complete. The results of the fracture analyses are compared in Figure 8. The three figures at the left side show the crack patterns from the drying structure modelled with continuum elements, whereas the three figures to the right show the results from the "softening" lattice analysis. It can be seen that the results are quite comparable. A better comparison can probably not be achieved because different element discretizations were used in the two models (viz. 464 triangular plane stress elements in the continuum analysis and 727 beams in the lattice analysis). It should be mentioned, that - because a softening fracture law was used – some of the cracks are not fully stress free, but are in a "softening" state. In the earlier lattice model, such beams would of course be immediately stress free because they would have been removed from the mesh completely. The good agreement between the two approaches is also clear from Figure 9, where the total deformation along the upper edge of the structure is plotted as a function of the drying time. Of course the good agreement was expected because the same flow equation and fracture model were used in the two models. The only difference was the finite element discretization, viz. plane stress elements and beams respectively.

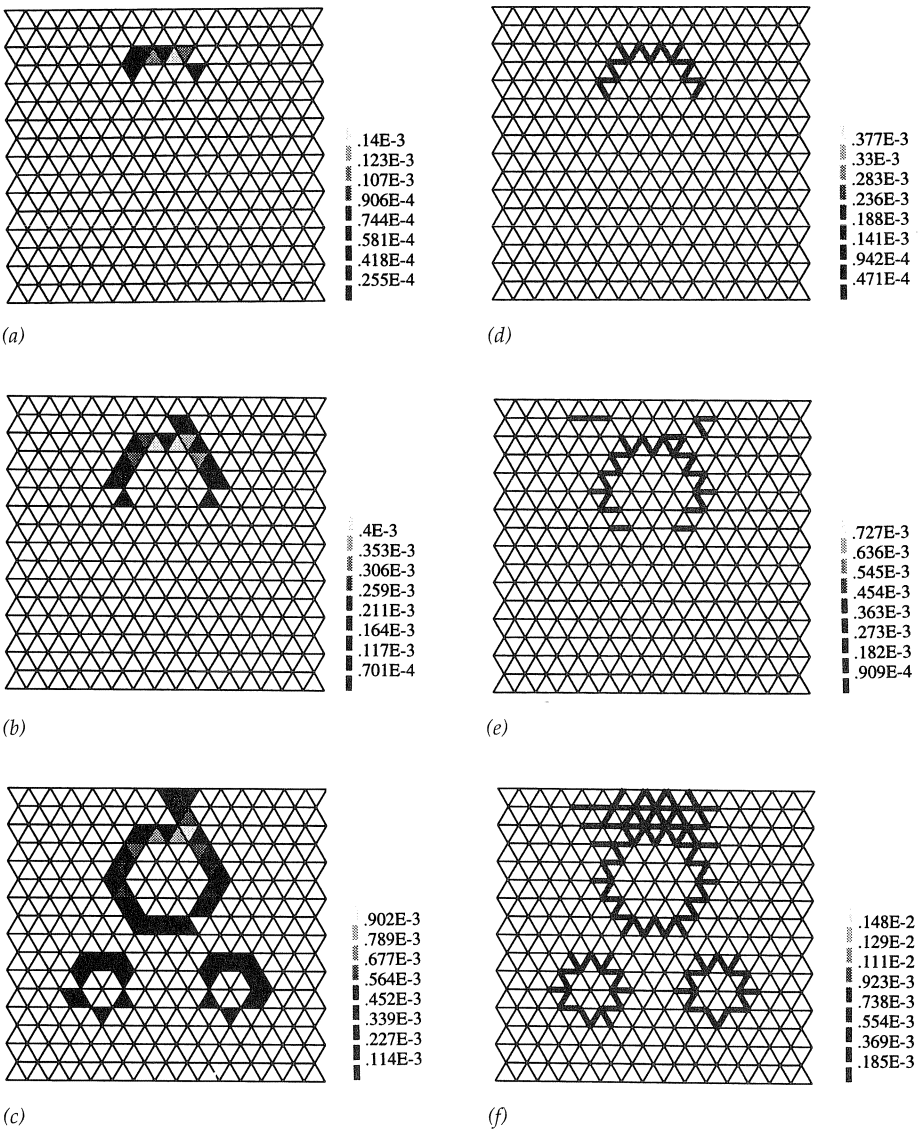

Fig. 8. Computed crack patterns from the continuum (smeared) crack approach following DIANA *(Figures a–c) and from the "softening" lattice mode (Figures d–f).*

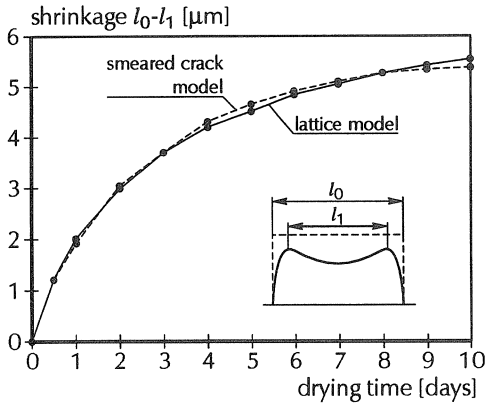

Fig. 9. Comparison of the total deformation along the top surface of the three particle structure of Fig. 7 for the continuum analysis and the "softening" lattice analysis.

6 Examples of hygral shrinkage cracking in different types of concretes

The lattice model has been applied for analyzing the shrinkage cracking in three different "numerical concretes". Two simulations concern normal gravel concrete containing dense impermeable aggregates. The third example concerns a lightweight concrete with porous lightweight aggregates. The difference between the two normal concrete simulations is in the variability and magnitude of the hygral shrinkage coefficient. In the examples the composite structure of Figure 1a was used. A relatively high convection coefficient was used (boundary condition 1), i.e. 3 mm/day. This corresponds to an immediate moisture equilibrium with the air at the drying surface, see Nilsson 1980 and Alvaredo 1994.

6.1 *Normal concrete 1*

The mechanical properties of the composite are shown in Table 2. Again a steep linear softening branch was assumed, and statistically distributed tensile strengths and Young's moduli of the matrix and interface zones were used.

Table 2. Mechanical properties for the fracture analysis of normal concrete 1.

	E [GPa]	υ [-]	α_{sh} [mm/(mm·h)]	f_t [MPa]	G_f [N/m]
aggregate	70 (-)	0.2	0.0	7.0	-
interface	12 (3)*	0.2	0.002	1.0 (0.25)	1.0 (0.0)
matrix	20 (4)	0.2	0.001	4.75 (1.25)	4.0 (0.0)

* values between parenthesis indicate the scatter of a given property.

The crack patterns at three different drying times are shown in Figure 10. The cracks are not immediately stress free, but are allowed to "soften". The figures indicate that cracking is initially confined to the interfacial regions. The total deformation along the top surface is compared to the results from a linear elastic analysis in Figure 11. Because cracks develop, the apparent total shrinkage deformation is now smaller than in the linear elastic analysis. Because relatively low values for α_{sh} were used, the differences between the linear elastic and the fracture analysis are relatively small.

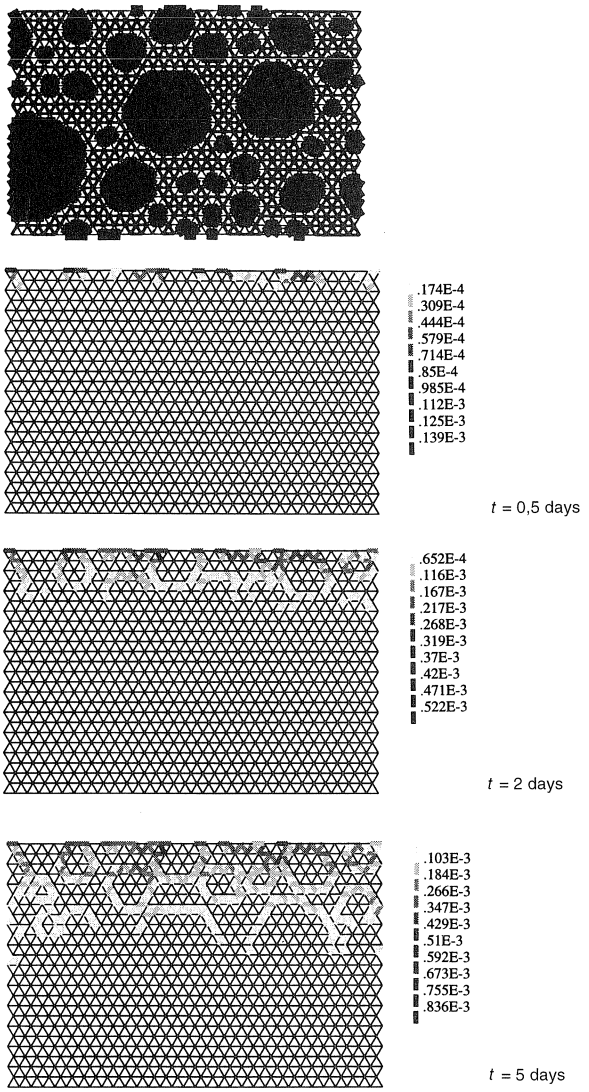

Fig. 10. Computed crack patterns from the "softening" lattice model for normal concrete 1 at three different drying times (t = 0.5, 2 and 5 days).

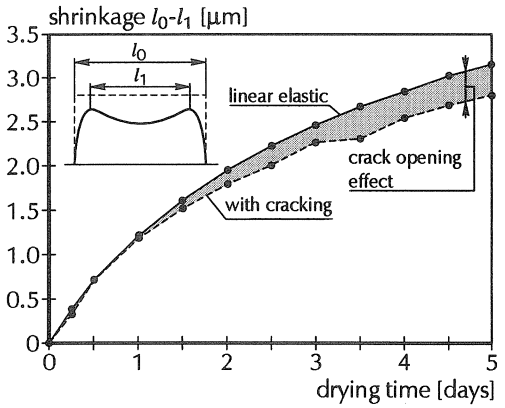

Fig. 11. Comparison of total shrinkage deformation along the upper surface of the composite structure (normal concrete 1) for the linear elastic analysis and the analysis where crack growth has been taken into account.

In the second analysis of normal concrete with higher values for α_{sh}, the differences are much larger, as will be shown next.

6.2 *Normal concrete 2*

In this example higher values for α_{sh} are chosen, which are given a random distribution as well. In Table 3, the various material parameters for this second simulation of shrinkage cracking in normal concrete are summarized. The aggregates are still assumed to be completely impermeable, whereas the matrix and interface are completely saturated at the beginning of the analysis.

Table 3. Mechanical properties for the fracture analysis of normal concrete 2.

	E [GPa]	υ [-]	α_{sh} [mm/(mm·h)]	f_t [MPa]	G_f [N/m]
aggregate	70 (-)	0.2	0.0	7.0	-
interface	12 (3)*	0.2	0.004 (0.001)	1.0 (0.25)	1.0 (0.0)
matrix	20 (4)	0.2	0.003 (0.002)	4.75 (1.25)	4.0 (0.0)

* values between parenthesis indicate the scatter of a given property.

Because of the higher shrinkage coefficients, cracking is now more severe. In Figure 12 the computed crack patterns are shown at two different drying times, namely at t = 1 and 4 days. For comparison the two crack patterns at t = 1 and 4 days for normal concrete 1 have been included in the same figure. Comparison reveals that now considerable matrix cracking occurs. It can be concluded that the hygral shrinkage coefficient is an important and sensitive parameter in such analyses.

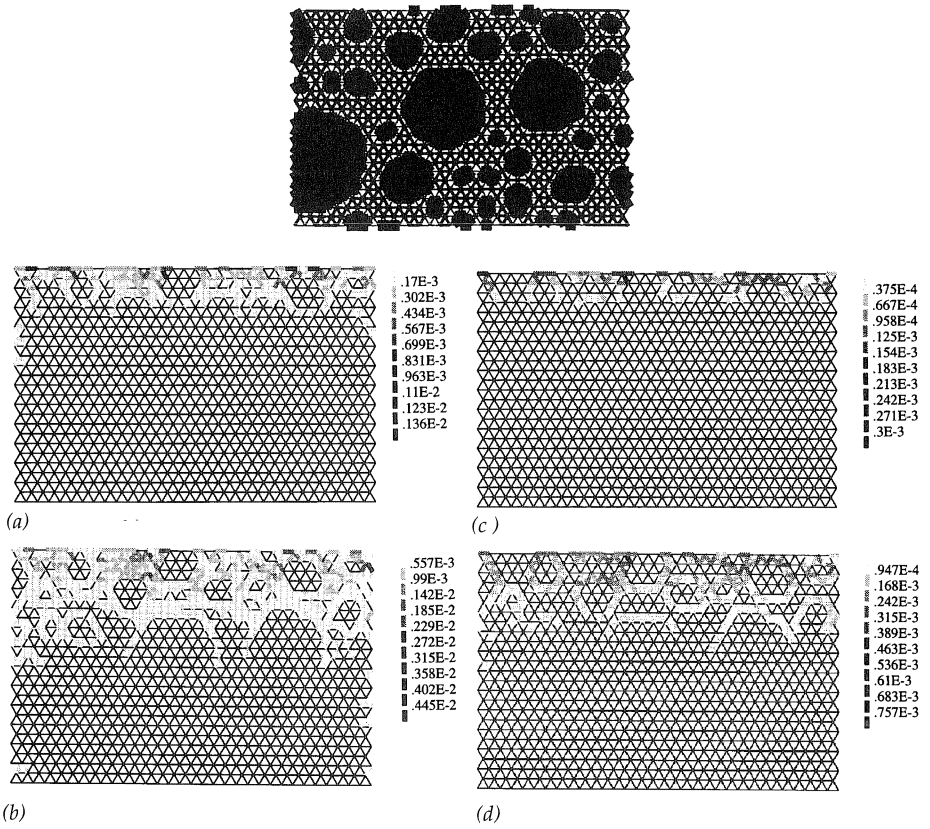

Fig. 12. Computed crack patterns from the "softening" lattice model for normal concrete 2 at t = 1 and 4 days (Figures a and b) and comparison to crack growth in normal concrete 1 at the same age (Figures c and d).

Future research should be directed to a sound experimental method for determining the hygral shrinkage coefficients of the mortar and interface zones. For the second normal concrete simulations, also the total deformation of the top surface has been compared to the deformation obtained from a linear elastic analysis. Figure 13 shows the result. The contribution from cracking is more pronounced as in the first normal concrete simulation (Figure 11), which demonstrates again the importance of the hygral shrinkage coefficient α_{sh}.

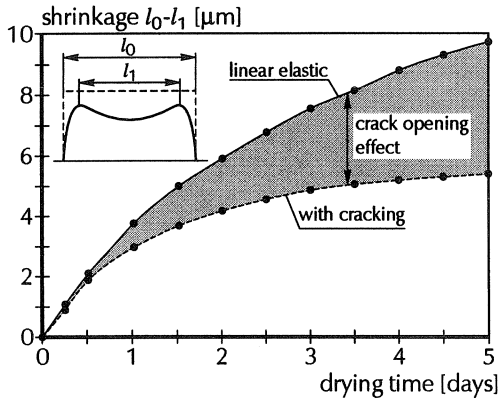

Fig. 13. Total shrinkage deformation for normal concrete 2, computed along the upper edge of the composite structure, using a linear elastic model and the "softening" lattice model.

6.3 *Lightweight concrete*

The third example concerns a "lightweight" concrete. The same properties are taken as for the normal concrete analysis 1, except that the Young's modulus of the aggregates is decreased by a factor 10, see Table 4. The aggregates are assumed to be impermeable, which means that the lightweight properties of the aggregates are reflected in the lower Young's modulus only. This makes this example perhaps a bit academic.

The drying crack patterns are shown in Figure 14 at three different times, viz. t = 0.5, 2 and 5 days. Crack growth seems now limited to the top surface only. The low Young's modulus of the aggregate material decreases the total stiffness of the structure, which leads to a higher shrinkage deformation as compared to normal concrete. In Figure 15 the total deformation of the upper edge of the structure is compared for the normal concrete 1 and lightweight concrete analyses. The increase of hygral shrinkage deformations in lightweight concrete is in agreement with experimental results and simplified analytical models (e.g. Hobbs 1971 and Picket 1947).

Table 4. Mechanical properties for the fracture analysis of lightweight concrete.

	E [GPa]	υ [-]	α_{sh} [mm/(mm·h)]	f_t [MPa]	G_f [N/m]
aggregate	7 (-)	0.2	0.0	7.0	-
interface	12 (3)*	0.2	0.002	1.0 (0.25)	1.0 (0.0)
matrix	20 (4)	0.2	0.001	4.75 (1.25)	4.0 (0.0)

* values between parenthesis indicate the scatter of that property.

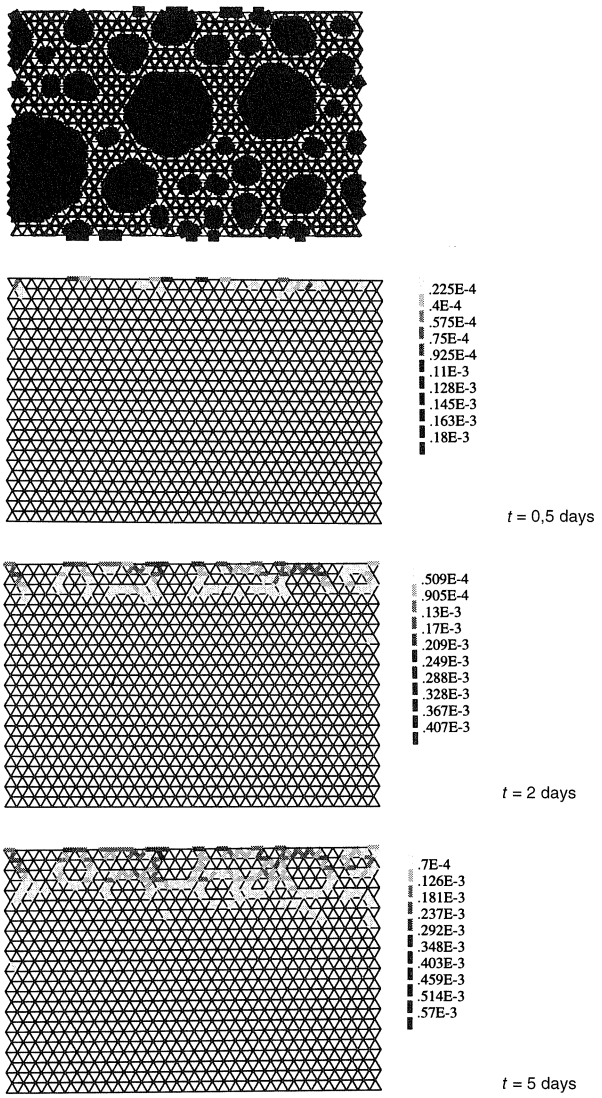

Fig. 14. Computed crack patterns from the "softening" lattice model for lightweight concrete at t = 0.5, 2 and 5 days.

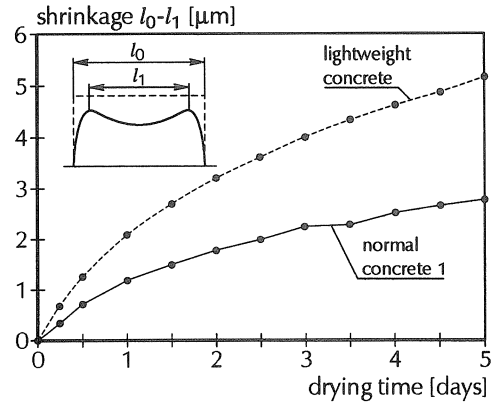

Fig. 15. Total shrinkage deformation for lightweight concrete, computed along the upper edge of the composite structure, using the "softening" lattice model. The lightweight concrete deformation is compared to the normal concrete 1 results.

7 Conclusions

The effect of drying shrinkage on crack growth in concrete composites has been studied by means of a numerical lattice model. In a lattice model, the material is discretized in a network of brittle breaking beam elements. Because the stress-deformation behaviour from lattice analysis are generally too brittle, a linear softening model was used for simulating crack growth. This is a large deviation from the earlier versions of the lattice model, in which a beam was completely removed after the stress exceeded the tensile strength of the material (Schlangen & Van Mier 1992). A moisture flow model was developed within the framework of the DIANA finite element package. The beams of the lattice are considered as conductive pipes for the flow analysis. The moisture flow model was described in detail in Sadouki & Van Mier 1996b, and only the main issues have been repeated in this paper. The results from the "lattice" flow analysis are in good agreement with the standard DIANA flow analysis. The subsequent fracture analysis with the "softening" lattice model compare very well to the results from a plane stress smeared crack analysis with DIANA. The shrinkage cracking in normal and lightweight concrete have subsequently been studied by means of the "softening" lattice model. The results reveal an important effect of the hygral shrinkage coefficient of the matrix and interfacial transition zone between aggregate and matrix. The amount of shrinkage cracks, as well as their location are highly dependent on the value of the hygral shrinkage coefficient. Experimental procedures for the determination of the hygral shrinkage coefficients for the matrix and interface zones should be subject of future research. Finally, simulations of shrinkage cracking in lightweight concrete reveal that the extent of cracking is less than for normal concrete, but because of the lower Young's modulus of the aggregates, a substantial increase of total shrinkage deformations is observed. This is in agreement with experimental observations.

In all, the modified lattice model seems a valuable tool for assessing the effect of hygral shrinkage cracking on the mechanical properties of concrete. In mechanical analyses such effects are normally neglected, but in view of the extent of cracking due to hygral shrinkage only, even after a few days of drying, the mechanical properties might be affected considerably. In tensile experiments on cement paste (Van Mier 1990), it was found that the shrinkage cracks have a significant effect on the final (mechanical) crack path.

Acknowledgement

The present study was made possible through a grant of the Netherlands School for Advanced Studies in Construction, the Ministry of Works in The Netherlands and ETH Zürich. The assistance of our colleagues at the Computational Mechanics Group at TNO Building Research is also gratefully acknowledged.

References

ALVAREDO, A.M. (1994), Drying shrinkage and crack formation, Building *Materials Reports No. 5*, AEDIFICATIO Publishers, IRB Verlag.

ARSLAN, A., SCHLANGEN, E. and VAN MIER, J.G.M. (1995), Effect of model fracture law and porosity on tensile softening of concrete, in *Proceedings FraMCoS-2*, Wittmann, F.H., Ed., AEDIFICATIO Publishers, Freiburg, 45.

BAŽANT, Z.P. and OH, B.-H. (1983), Crack band theory for fracture of concrete, *Materials & Structures (RILEM)*, **16**, 155.

DIANA (1995), *Users manual - Release 6.1*, Diana Analysis BV, Delft, The Netherlands.

HILLERBORG, A., MODÉER, M. and PETERSSON, P.-E. (1976), Analysis of crack formation and crack growth in concrete by means of fracture mechanics and finite elements, *Cem. & Conc. Res.*, **6**, 773.

HOBBS, D.W. (1971), The dependence of the bulk modulus, the Young's modulus, creep, shrinkage and thermal expansion of concrete upon aggregate volume concentration, *Materials & Structures (RILEM)*, **4**(20), 107–114.

MARTINOLA, G. and WITTMANN, F.H. (1995), Application of fracture mechanics to optimize repair mortar systems, in *Proceedings FraMCoS-2*, Wittmann, F.H., Ed., AEDIFICATIO Publishers, Freiburg, 1481.

NILSSON, L.O. (1980), Hygroscopic moisture in concrete drying, measurements and related material properties, *Report TVBM-1003*, Lund Institute of Technology, Sweden.

PICKET, G. (1946), Shrinkage stresses in concrete, *J. Amer. Conc. Inst.*, **17**(4), pp. 165–195 and 361–398.

QUENARD, D. and SALLEE, H. (1992), Water vapour adsorption and transfer in cement-based materials: a network simulation, *Materials & Structures (RILEM)*, 25, 515.

ROELFSTRA, P.E., SADOUKI, H. and WITTMANN, F.H. (1985), Le béton numérique, *Mater. Struct. (RILEM)*, **18**, 327.

SADOUKI, H. and VAN MIER, J.G.M. (1996a), Simulation of hygral crack growth in concrete repair systems, Submitted for publication in *Materials & Structures (RILEM)*.

SADOUKI, H. and VAN MIER, J.G.M. (1996b), Meso-level analysis of moisture flow in cement composites using a lattice type approach, Submitted for publication in *Materials & Structures (RILEM)*.

SCHLANGEN, E. and VAN MIER, J.G.M. (1992), Experimental and numerical analysis of micro-mechanisms of fracture of cement-based composites, *Cem. & Conc. Composites*, **14**, 105.

SCHLANGEN, E. (1993), Experimental and numerical analysis of fracture processes in concrete, *Ph.D. thesis*, Delft University of Technology, The Netherlands.

SCRIVENER, K. (1989), The microstructure of concrete, in *Materials Science of Concrete I*, Skalny, J. Ed., The American Ceramic Society Inc., Westerville, OH, 127.

VAN MIER, J.G.M. (1986), Fracture of concrete under complex stress, HERON, **31**(3). 254.

VAN MIER, J.G.M. (1990), Mode I behaviour of concrete: Influence of the rotational stiffness outside the crack zone, in *Analysis of Concrete Structures by Fracture Mechanics*, Elfgren, L. and Shah, S.P., Eds., Chapman & Hall, London/New York, 19.

VAN MIER, J.G.M.. SCHLANGEN, E. and VERVUURT, A. (1995), Lattice type fracture models for concrete, in *Continuum Models for Materials with Microstructure*, Mühlhaus, H.-B., Ed., John Wiley & Sons Ltd., Chap. 10.